21 April 2009 Volume 130 Number 15

THE JOURNAL OF CHEMICAL PHYSICS

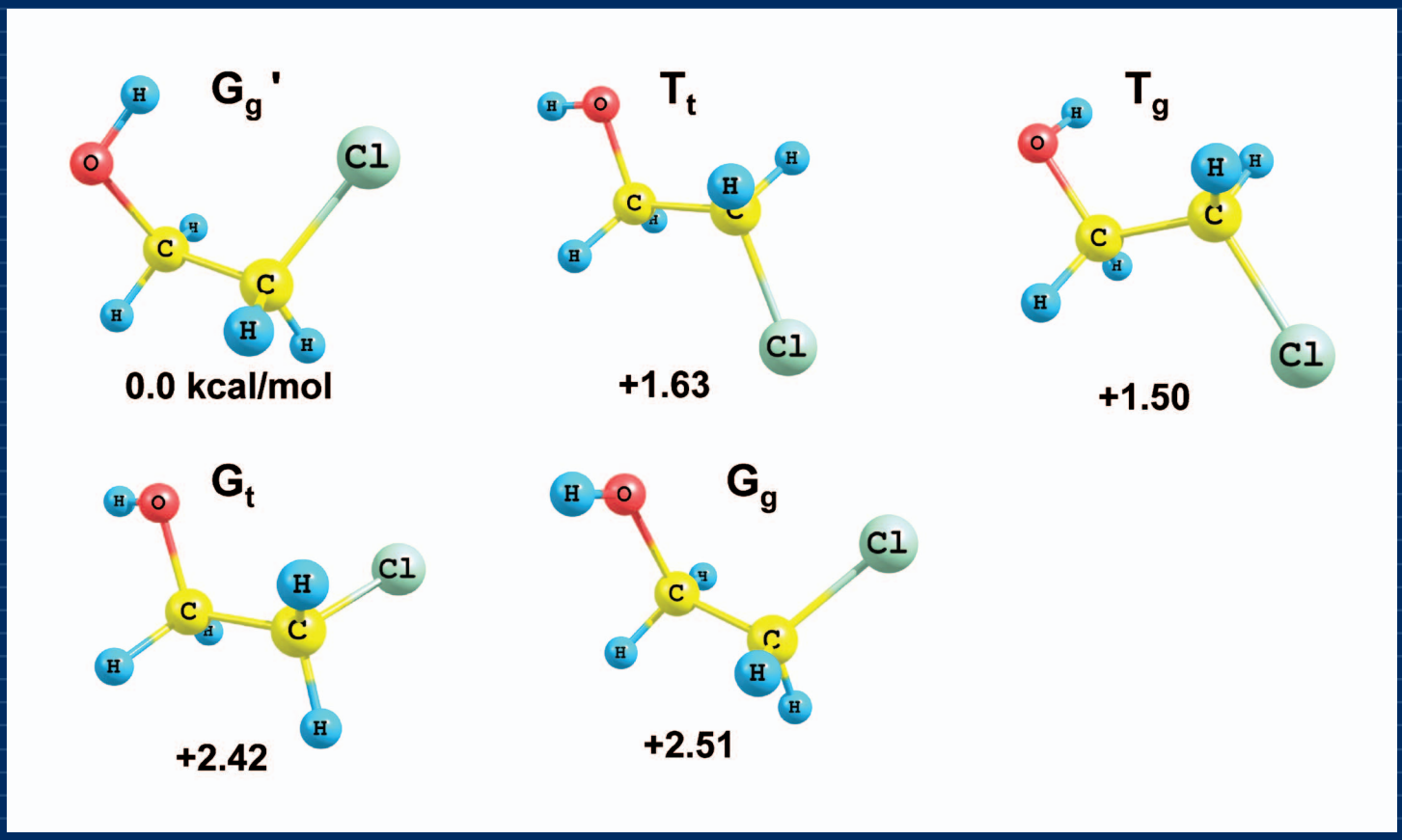

AMERICAN INSTITUTE OF PHYSICS

Nanoporous silica-water interfaces studied by sum-frequency vibrational spectroscopy

Luning Zhang,[1,a)] Seema Singh,[2,b)] Chuanshan Tian,[1] Y. Ron Shen,[1,c)] Yan Wu,[3] Mark A. Shannon,[3] and C. Jeffery Brinker[2,4]
[1]*Physics Department, University of California, Berkeley, California 94720, USA*
[2]*Sandia National Laboratories, Albuquerque, New Mexico 87185, USA*
[3]*Department of Mechanical Science and Engineering, University of Illinois, Urbana, Illinois 61801, USA*
[4]*Department of Chemical and Nuclear Engineering, University of New Mexico, Albuquerque, New Mexico 87131, USA*

(Received 20 October 2008; accepted 16 March 2009; published online 21 April 2009)

Using sum-frequency vibrational spectroscopy, we found that water structure at nanoporous silica/water interfaces depended on the nanoporous film structure. For a periodic, self-assembled nanoporous film with monosized 2 nm pores occupying 20% of the top surface area, the surface vibrational spectrum was dominated by water in contact with silica, bare or covered by silane, at the top surface. It resembled the spectral characteristic of the hydrophilic water/silica or the hydrophobic water/silane interface. For a fractal nanoporous film with pores ranging from 5 to 50 nm in size occupying 90% of the top surface, the spectrum for a trimethyl silane-coated superhydrophobic porous film resembled largely that of a water/air interface. Only when the silane was completely removed would the spectrum revert to that characteristic of a hydrophilic water/silica interface. The surface charging behaviors of the bare nanoporous films in water with different *p*H were monitored by spectroscopic measurements and atomic force microscopy force measurements. The point of zero charge for the periodic porous film is around *p*H 2, similar to that of the flat silica surface. The point of zero charge could only be determined to be $p\mathrm{H} < 6$ for the fractal porous film because the thin fractal solid network limited the amount of surface charge and therefore, the accuracy of the measurements. © *2009 American Institute of Physics*. [DOI: 10.1063/1.3118906]

I. INTRODUCTION

Water interfaces with nanostructured materials have attracted much attention in recent years.[1–9] Interesting phenomena such as preferential ion adsorption in pores,[1,2] unique single-molecule diffusion patterns,[3] gate-controlled ion transport,[4,5] high-sensitivity ion sensing,[6–8] and enhanced streaming current in nanochannels[9] have been reported. The case of the water/porous-silica interface is particularly interesting. It is known that a bare nanostructured silica surface is hydrophilic, but when silica is covered by silane, the surface can be rendered hydrophobic and even superhydrophobic (SH). Both the hydrophobic silane termination and the geometrical nanostructure of the surface contribute to the surface hydrophobicity.[10,11] The SH nanostructured surfaces are interesting not only because of their importance for basic understanding of hydrophilicity and hydrophobicity, but also because of their potential applications in fabricating self-cleaning surfaces,[12,13] designing low-friction coatings,[14] and mimicking biosurfaces.[15–17] Surface roughness effect on wetting may also find relevance to water-membrane interactions for water purification and desalination[18,19] and capillary evaporation, which could influence protein folding and "nano-bubble-gated" transport in natural molecular and ion channels.[20,21]

On a nanostructured surface, water can be in the so-called Wenzel[22] or Cassie state.[23] In the Wenzel state, water fills the nanopores and is in direct contact with silica, and in the Cassie state, air is supposed to be trapped in nanopores and water is only in contact with silica at the top surface. It is also possible that water is in a mixed "Cassie–Wenzel" state with water partially filling nanopores, depending on the coverage of silane and geometry of the surface nanostructure.[24,25] Most information about such interfaces has been derived from water contact angle (CA) and neutron reflection measurements.[25] At the present time, very little is known about the molecular structure of water at such interfaces. This is because there are not many easily assessable analytical tools for studying the microscopic structures of buried interfaces. Sum-frequency vibrational spectroscopy (SFVS) is unique in its ability to generate vibrational spectra for solid/water interfaces and seems ideally suited for probing the water interfacial structure of nanoporous silica surfaces.

We have used SFVS to study water interfaces with two types of nanoporous silica films, one consisting of a periodic

[a)]Present address: Molecular Physics Laboratory, SRI International, Menlo Park, CA 94025. Electronic mail: luning.zhang@sri.com.
[b)]Present address: Sandia National Laboratory, Livermore, CA 94550. Electronic mail: seesing@sandia.gov.
[c)]Author to whom correspondence should be addressed. Electronic mail: yrshen@calmail.berkeley.edu.

pattern of ~2 nm diameter pores having a silica/pore area ratio of 4:1 at the top surface,[26] and one with a fractal nanoporous structure having a silica/pore area ratio of 1:10 at the top surface.[25] Spectra observed in the OH stretch region were to be compared with those of water/vapor,[27] water/silica,[28,29] and water/silane-covered-silica interfaces. Hydrophobicity of the nanoporous films, described by the water CA, was altered by changing the relative coverage of trimethyl silane $Si-O-Si(Me)_3$ using a dose-dependent UV-ozone treatment.[30,31] For each system, the corresponding spectral change provided information on how the interfacial water structure varied with change in hydrophobicity (while the morphology of the surface nanostructure remained unchanged). We also studied how *p*H variation affected the spectra of bare nanoporous films and thus, deduced information about their surface charging behaviors. To further check the charging behaviors, we carried out atomic force microscopy (AFM) force measurements on the films using a colloidal probe with a 5 μm silica sphere at the end of the cantilever.[32] The results agreed qualitatively with those deduced from SFVS.

We found that for the water interface with the bare periodic nanoporous film, the sum-frequency (SF) vibrational spectral profiles were similar to those of the water/quartz interface.[28,29] Its surface charging behavior with a point of zero charge (p.z.c.) near *p*H 2 was also similar to that of the water/silica interface,[28,29] as one would expect from the large contact area of water with silica at the top surface. For the same reason, when the periodic nanoporous film was covered with silane, the spectra appeared similar to those of water/octyltrichlorosilane (OTS)-coated silica interface (water/OTS). Pores, on the other hand, dominate the top surface of the fractal nanoporous film. When silica was covered with silane, the observed spectra of the water/SH film interface resembled those of the water/vapor interface, suggesting that the water interface is in the Cassie state with air trapped in the pores. Stepwise removal of the silane coating reduced the hydrophobicity, changing the interface from the Cassie state to the Cassie–Wenzel mixed state and then eventually, becoming hydrophilic with complete wetting. However, even in the highly hydrophilic case with CA down to 10°, the spectrum still has pronounced characteristic features of water/vapor interface, including the presence of the free OH peak. The *p*H effect on the water interface with the bare fractal film was hard to detect until the *p*H was increased above 7. With a smaller fraction of the silica area occupying the top surface, relatively weak deprotonation of silica was not expected to cause significant change in the net polar orientation of the interfacial water molecules, which makes determination of the p.z.c. difficult. All we could deduce was that the p.z.c. was less than *p*H 7. Addition of salt into the solution did not change the spectrum or the AFM result appreciably when *p*H was below 7, also only suggesting that the p.z.c. was below *p*H 7.

In the following, we will briefly describe the theoretical background for SFVS and experimental setup, followed by the presentation of spectra, AFM data analysis, and discussion of results for various water interfaces with nanoporous films.

II. THEORETICAL BACKGROUND

The theoretical background of SFVS for surface and interface studies has been described in detail elsewhere.[33–35] For SF generation from overlapping of a visible input with intensity I_1 and fixed frequency ω_1 and an IR input with intensity I_2 and tunable frequency ω_2 at an interface, the SF signal is given by[33]

$$S(\omega=\omega_1+\omega_2)\propto|[\vec{\vec{L}}(\omega)\cdot\hat{e}]\cdot\vec{\vec{\chi}}_S^{(2)}:[\hat{e}_1\cdot\vec{\vec{L}}(\omega_1)]\times[\hat{e}_2\cdot\vec{\vec{L}}(\omega_2)]|^2 I_1 I_2=|\vec{\vec{\chi}}_{\mathrm{eff}}^{(2)}|^2 I_1 I_2, \quad (1)$$

where $\hat{e}_i$ and $\vec{\vec{L}}(\omega_i)$ denote, respectively, the unit polarization vector and the tensorial Fresnel transmission coefficient at ω_i, and $\vec{\vec{\chi}}_S^{(2)}$ is the surface nonlinear susceptibility tensor. In this paper, spectra are presented as $|\vec{\vec{\chi}}_S^{(2)}(\omega_2)|^2$ after removing the Fresnel factors in Eq. (1). (The expression for the Fresnel factor can be found in Ref. 36. The refractive indices at 532 nm are taken as 1.461 for silica and 1.335 for water. The refractive index of the porous interfacial layer is calculated by taking the average of silica and water based on their volume fraction. The refractive index of water in the OH stretching region was obtained from Ref. 37.) When ω_2 is near a continuum of vibrational resonances, $\vec{\vec{\chi}}_S^{(2)}$ can be expressed as

$$\vec{\vec{\chi}}_S^{(2)}=\vec{\vec{\chi}}_{\mathrm{NR}}^{(2)}+\int\frac{\vec{\vec{A}}_q\rho(\omega_q)}{\omega_2-\omega_q+i\Gamma_q}d\omega_q. \quad (2)$$

Here, $\vec{\vec{\chi}}_{\mathrm{NR}}^{(2)}$ describes the nonresonant contribution. $\vec{\vec{A}}_q$, ω_q, and Γ_q represent the amplitude, frequency, and damping constant of the q^{th} vibrational resonance, respectively, and $\rho(\omega_q)$ is the density of modes at ω_q. For discrete resonances, Eq. (1) reduces to

$$\vec{\vec{\chi}}_S^{(2)}=\vec{\vec{\chi}}_{\mathrm{NR}}^{(2)}+\sum_q\frac{\vec{\vec{A}}_q}{\omega_2-\omega_q+i\Gamma_q}. \quad (3)$$

The amplitude $A_{q,ijk}$ in the laboratory coordinates (x,y,z) is related to its counterpart $a_{q,lmn}^{(2)}$ of the molecular hyperpolarizability in the molecular coordinates (ξ,η,ζ) through a coordinate transformation and an average over the molecular orientational distribution $f(\Omega)$,

$$A_{q,ijk}=N_S\int a_{q,lmn}(\hat{i}\cdot\hat{l})(\hat{j}\cdot\hat{m})(\hat{k}\cdot\hat{n})f(\Omega)d\Omega, \quad (4)$$

which vanishes under electric-dipole approximation if $f(\Omega)$ has inversion symmetry.

Because $\chi_S^{(2)}(\omega_2)=|\chi_S^{(2)}|(\omega_2)\exp[i\Phi(\omega_2)]=\mathrm{Re}\,\chi_S^{(2)}+i\,\mathrm{Im}\,\chi_S^{(2)}$ is complex, measurement of $S(\omega=\omega_1+\omega_2)$ [or $|\chi_S^{(2)}(\omega_2)|$] only is not sufficient to determine $\vec{\vec{\chi}}_S^{(2)}$.[29] Even in cases where a spectrum of $|\chi_S^{(2)}(\omega_2)|$ can be approximated by discrete resonances, fitting of the spectrum by Eq. (3) is not necessarily unique unless signs of $\vec{\vec{A}}_{q,ijk}$ are known. To completely characterize the resonances in the spectrum of $|\vec{\vec{\chi}}_S^{(2)}|$, it is necessary to determine the phase of $\vec{\vec{\chi}}_S^{(2)}$ independently by measurement. This is particularly important for water interfaces, as has been demonstrated recently.[27–29,38] A spectrum of $\mathrm{Im}\,\vec{\vec{\chi}}_S^{(2)}$, being analogous to Im ε for linear absorp-

tion spectrum with ε denoting the optical dielectric constant, offers direct information on spectral resonance. Following Eqs. (2) and (3), we have, respectively,

$$\mathrm{Im}\ \vec{\vec{\chi}}_S^{(2)} = \int \frac{\vec{\vec{A}}_q \rho(\omega_q)\Gamma_q}{(\omega_2 - \omega_q)^2 + \Gamma_q^2} d\omega_q \tag{5}$$

and

$$\mathrm{Im}\ \vec{\vec{\chi}}_S^{(2)} = \sum_q \frac{\vec{\vec{A}}_q \Gamma_q}{(\omega_2 - \omega_q)^2 + \Gamma_q^2}. \tag{6}$$

In our study of interfacial water structure at water/porous-silica interfaces, the SF spectrum comes mainly from net polar orientations of various water species. At different *p*H values, the silica surface can be deprotonated (or protonated if *p*H is sufficiently low), leaving the surface negatively (or positively) charged. The deprotonated surface can change the bonding geometry of water molecules adsorbed at the surface and the surface field created by the surface charges can reorient the more loosely bonded water molecules at the interface. Thus, in general, we can express the surface susceptibility as[39–41]

$$\vec{\vec{\chi}}_S^{(2)} = \vec{\vec{\chi}}_{S0}^{(2)} + \Delta\vec{\vec{\chi}}_S^{(2)}, \tag{7}$$

with $\vec{\vec{\chi}}_{S0}^{(2)}$ denoting the surface susceptibility of the neutral surface, and $\Delta\vec{\vec{\chi}}_S^{(2)}$ the change resulting from deprotonation (or protonation). The bulk *p*H value at which a surface appears neutral is known as the p.z.c. At the p.z.c., $\Delta\vec{\vec{\chi}}_S^{(2)}=0$ (Refs. 42 and 43) and the addition of salt into the aqueous solution should not change the interfacial structure or $\vec{\vec{\chi}}_S^{(2)}$ because ions would not be attracted to the interfacial region. The p.z.c. is, therefore, also identified as the point of zero salt effect. A flat fused silica surface is known to have a p.z.c. near *p*H 2. It would be important to know whether porous silica surfaces would have different p.z.c. values.

III. EXPERIMENTAL ARRANGEMENT

The experimental setups for SFVS and the phase measurement were described elsewhere.[36,38,44,45] Briefly, a picosecond Nd:yttrium aluminum garnet laser/optical parametric system was used to generate the visible input at 532 nm and the tunable IR input pulses that overlapped at the sample. The SF signal recorded in the reflected direction was normalized against that from a z-cut α-quartz crystal. Phase measurements were carried out by the interference scheme described in Refs. 27 and 36. The phase of $\vec{\vec{\chi}}_S^{(2)}$ was derived from interference of the SF signal with that from a nonresonant reference sample.

The AFM force measurements were carried out on an Asylum Research MFP3 atomic force microscope. A standard V-shape silicon nitride cantilever with a nominal spring constant of 0.06 N/m from Novascan Technologies and a silica sphere (5 μm diameter) at the AFM tip was used as the probe. The silica sphere was nonporous. Before each measurement, the silica colloidal probe was treated with oxygen plasma inside the chamber of a molecular vapor deposition (MVD 100) machine (Applied MicroStructures). The oxygen plasma procedure eliminates organic contamination and ensures a high density of silanol groups on the silica probe. The spring constant of the cantilever was calibrated using the thermal noise method, where the power spectrum of the cantilever thermal fluctuation in air was fitted using a simple harmonic oscillator model.[46,47] The force between the sample surface and the colloidal probe was sensed by the cantilever deflection as two surfaces were brought into contact. The electrostatic component of the force can be related to the surface charge on the sample, as we shall discuss later.

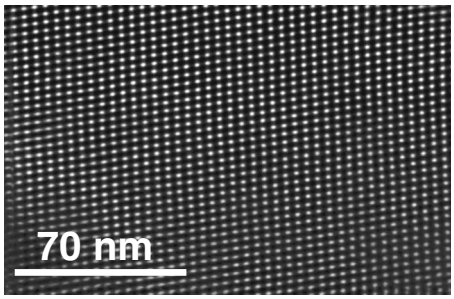

FIG. 1. TEM image of a periodic nanoporous film. The dark region is silica and the bright region is air.

The nanoporous samples used in our study were films coated on silica substrates. Two types of nanoporous films, periodic and fractal, were studied. The periodic nanoporous silica films were prepared on silica substrates by the so-called evaporation-induced self-assembly method[48] following the procedure described in Ref. 26. Figure 1 shows the results of transmission electron microscopy (TEM) image on such a film. The pores formed a face-centered-cubic lattice structure and were interconnected by thin necks. The pore diameter was ~2 nm and the spacing between neighboring pores was 2 nm, leading to an area ratio of pores versus solid of 1:4 on the top surface. This film exhibited excellent mechanical strength and thermal stability. The periodic porous films could be made hydrophobic by exposing the surface to hexamethyldisilizane (HMDZ) vapor for 30 min to replace H of the silanol groups by $Si(CH_3)_3$ on the surface via silanation. The water CA on such hydrophobic surfaces was determined to be approximately 90°.

Fractal nanoporous films were prepared following the procedure described in Ref. 25, which was a variation in the method developed by Prakash *et al.*[49] Figure 2 displays a TEM image and an AFM surface topography image of such a film. The dark region in the TEM image is the silica skeleton of the film, and the bright region is air. The film had a bulk porosity of ~85% (with ~15% of the space filled by silica). Due to the fractal nature, the solid fraction is a very small ratio of the top surface area. We estimated a surface porosity of ~90% at the water/fractal film interface. The pore size ranged from 5 to 50 nm. The AFM image showed a surface root-mean-square roughness of about 12.4 nm. The film was fragile but could withstand normal water rinsing and dry nitrogen jet cleaning. The as-deposited hydrophobic film could be made SH by exposing it to HMDZ, and the water CA of the film consistently reached 160°–165°.

UV/ozone treatment was effective to photocalcine the

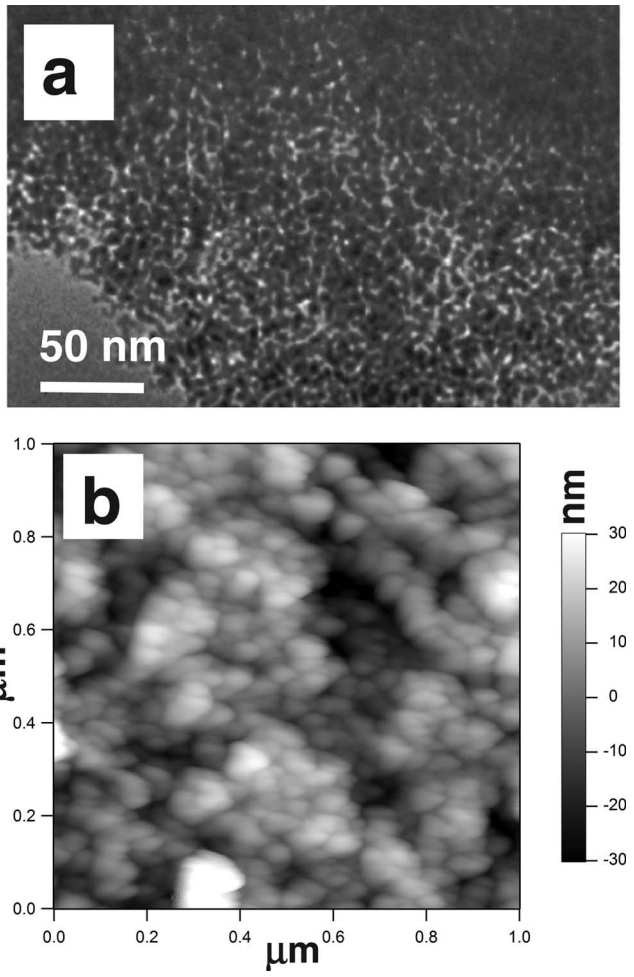

FIG. 2. (a) TEM image and (b) atomic force microscope topography of a fractal nanoporous film. In (a), the dark region is silica and the bright region is air. In (b), the surface root-mean-square roughness of the film is about 12.4 nm.

silane groups on the nanoporous films and alter the hydrophobicity.[30,31] A high-pressure mercury lamp (UVP, CPQ-8030) with about 30 mW/cm^2 power was applied and used on the films. Controlling the time of exposure controlled the surface density of the $-CH_n$ and $-CF_n$ groups remaining on the surface, thereby, changing the hydrophobicity. In several recent studies,[50,51] the UV photocalcination procedure was found to be able to preserve the silica skeletal while removing the surface surfactants and silane groups in a controlled fashion until all the organic molecules were calcined. The photocalcination reaction mechanism has also been proposed.[31,50]

In the study of water interfaces with nanoporous films, we used water/vapor, water/silica, and water/OTS interfaces as references. The hydrophilic fused silica surface was prepared by the usual cleaning method,[45] and the OTS-coated sample was prepared following the method of Sagiv.[52] The *p*H variation (from 9 to 3) was achieved by titration of a 5 mM NaOH solution. Average of *p*H readings on a digital *p*H meter (Accumet, Fisher Scientific) before and after each SFVS or AFM measurement was taken as the recorded *p*H values.

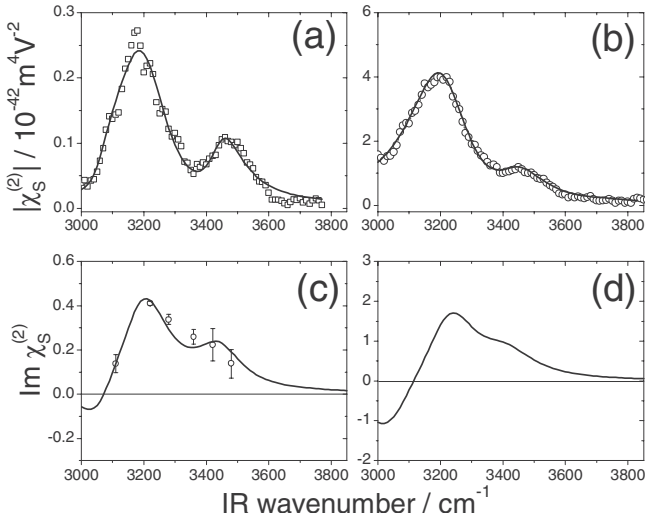

FIG. 3. SSP-SF vibrational spectra of (a) the water/periodic nanoporous silica interface and (b) the water/silica interface. The corresponding Im $\chi_S^{(2)}$ spectra are shown, respectively, in (c) and (d). The solid curves were obtained from Eq. (6) using the parameters deduced for the discrete resonances from fitting the spectra in (a) and (b) with Eq. (2). The discrete dots are data points obtained directly from SFVS phase measurements. Purified water with a resistivity of 18.3 MΩ cm was used.

IV. RESULTS AND DISCUSSION

A. Periodic nanoporous film

Presented in Fig. 3 is the SF intensity spectrum with SSP input/output polarization combinations obtained from the interface of water (*p*H=5.8) with a fully calcined periodic porous film. The spectrum of the reference water/silica interface is also shown for comparison in Fig. 3. The SPS spectra were much weaker and less informative and are not presented here. We notice that the two spectra in Figs. 3(a) and 3(b) are very similar. Both exhibit the characteristic liquidlike and icelike features at 3450 and 3200 cm^{-1}, respectively. It suggests that water molecules neighboring silica must have dominated the spectra. The spectrum for the water/periodic porous film interface, however, is only about 5% as intense as for the water/silica interface (corresponding to a ratio of 0.22:1 in $|\chi_S^{(2)}|$), although the TEM image indicates an area ratio of silica to pores of 4:1 on the top surface of the porous film. This is probably because the silica part of the top surface was not flat, especially around the edges of the pores. Water molecules adsorbed on it could have a rather wide angular spread, and orientational averaging over the distribution could greatly reduce the SFVS signal. Inside the pore region, water molecules are likely to have wetted the walls of the pores, but their wide orientational distribution would contribute little to the SF spectra. The absence of the dangling OH peak at 3700 cm^{-1} suggests essentially nonexistence of hydrophobic interfacial areas.

In our spectral analysis, we approximated the SSP water interfacial spectra by discrete resonances. We followed the procedure described in Ref. 41 for the water/alumina interfaces. The spectra could be fit using Eq. (1) by discrete resonances at 3420, 3220, and 3040 cm^{-1} with bandwidths (full width at half maximum) of ~200, 200, and 180 cm^{-1}, respectively. From the phase measurement, the signs of their

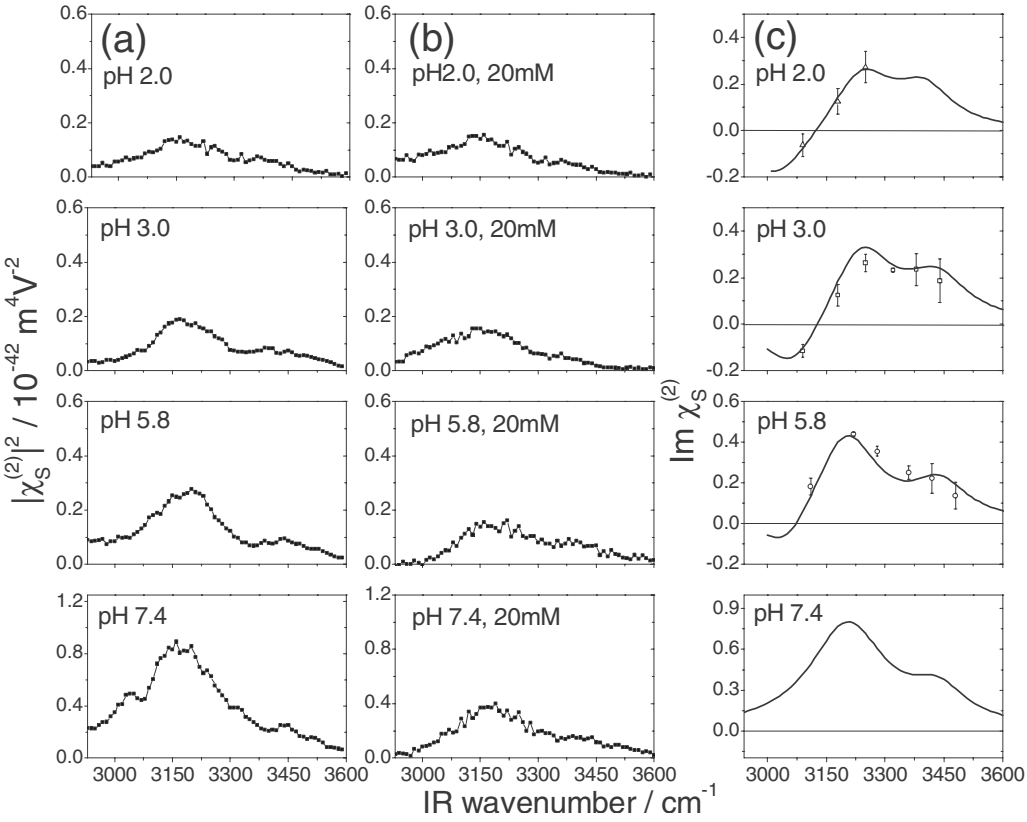

FIG. 4. SSP spectra for the water/periodic nanoporous silica interface at different solution *p*H: (a) without electrolyte and (b) with electrolyte (20 mM NaCl). (c) Im $\chi_S^{(2)}$ spectra associated with the $|\chi_S^{(2)}|^2$ spectra in (a). The solid curves were obtained from Eq. (6) using the characteristic parameters deduced for the discrete resonances from fitting the spectra in Fig. 3. The dots are data points obtained directly from SFVS phase measurements. The film was not covered by silane.

amplitudes were found to be positive, positive, and negative, respectively. The fitting result then led to the corresponding Im $\chi_S^{(2)}$ spectra.[53] Figures 3(c) and 3(d) display the SSP Im $\chi_S^{(2)}$ spectra, associated with those presented in Figs. 3(a) and 3(b), for interfaces of water/periodic nanoporous film and water/silica, respectively. The two Im $\chi_S^{(2)}$ spectra are again similar except for the intensity as expected. Thus, for the periodic nanoporous film, the water interfacial structure in the water-silica contact area of the top surface must be essentially the same as that of the water/silica interface.[28,29,37]

The spectrum for the interface of water and a bare periodic nanoporous film varies with *p*H. Figure 4 shows the SSP spectra of $|\chi_S^{(2)}|^2$ and Im $\vec{\chi}_S^{(2)}$ at different *p*H values. They appear very similar to those observed from water/quartz interfaces[28,29] except that their intensities are lower. Thus, the interpretation of how water structure at the water/quartz interface changes with *p*H described in Ref. 29 also applies to the case of porous silicate here. Briefly, water molecules adsorbed at the interface form a disordered H-bonding network with some local icelike tetrahedral bonding. The liquidlike band centered at 3420 cm^{-1} is attributed to the more disordered and loosely bonded water molecules, and the icelike band centered at ~3200 cm^{-1} to the more-ordered and tightly bonded water molecules. Increasing *p*H deprotonates more of the hydrogenated silica surface. It alters the distribution of water molecules with different bonding geometries to the silica surface. The more negative surface charge also creates a stronger negative surface field that could reorient more interfacial water molecules with O–H pointing toward the interface. At low *p*H(~2), the silica surface is neutral; water species contributing to the negative icelike band in the Im $\vec{\chi}_S^{(2)}$ spectrum have a net polar orientation of O–H pointing away from the interface, and those contributing to the positive liquidlike band have O–H pointing toward the interface. At high *p*H, the negative surface field reorients the interfacial water molecules leading to decrease and increase in the net polar orientations of molecules contributing to the icelike and liquidlike bands, respectively. Finally, with further increase in *p*H, the net polar orientation of the water species responsible for the icelike band first reduces to zero and then flips to have average dipoles pointing toward the interface. The overall spectral intensity is significantly higher at high *p*H. Neutrality of the surface at *p*H=2 was confirmed by adding salt into the aqueous solution. As seen in Fig. 4, addition of 20 mM of NaCl changes appreciably the spectra of *p*H=3 or higher, but not the one at *p*H=2. Therefore, the p.z.c. for the periodic porous silica can be set at *p*H~2, close to that of the flat silica surface.[28,54]

The AFM force measurement over a surface also allows the deduction of an effective charge density at the surface (see detailed description and derivation in the Appendix). Figure 5 shows the effective surface charge densities on the periodic nanoporous film and the flat silica surface versus solution *p*H. For both surfaces, the magnitude of the negative effective surface charge density increases with *p*H because

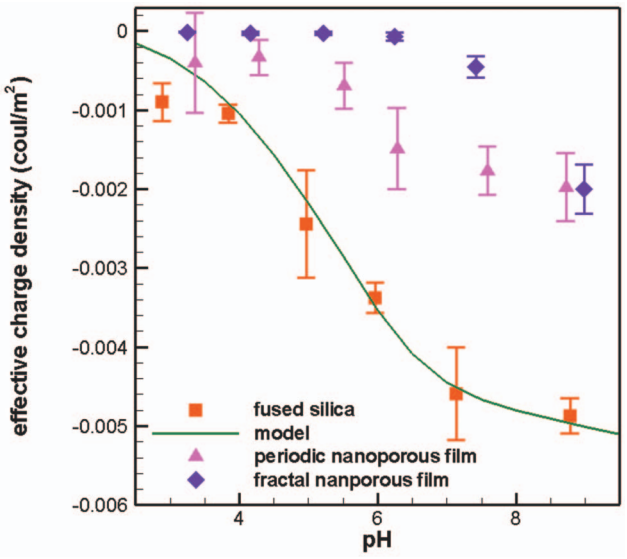

FIG. 5. (Color) Effective surface charge density vs solution *p*H for fused silica, periodic nanoporous silica film, and fractal nanoporous silica film immersed in water. The solid line shows the model prediction for the fused silica case assuming the silica colloidal probe has the same degree of deprotonation as the fused silica surface.

of deprotonation of the surfaces. The negative surface charge is smaller on the periodic porous film versus the flat fused silica surface due to a smaller effective contact area, but the overall trend is similar for the two surfaces. The p.z.c. for the periodic porous film may appear to be somewhat larger, but this could be the result of noise in the measurements, particularly at lower *p*H where a lower surface charge exerts a lower force.

Covering the periodic nanoporous film with trimethyl silane makes the film hydrophobic. Our sample prepared by exposing the surface to HMDZ had a water CA of 90°. The intensity spectra of its interface with water are displayed in Fig. 6. For comparison, the spectra of partially photocalcined film (with CA ~ 40°) with water as well as those of the hydrophobic water/OTS interface are also presented in Fig. 6. It is seen that the spectrum for the CA ~ 90° interface resembles that of the water/OTS interface except that the spectral intensity is reduced by ~75%. This is expected knowing that the spectrum should be dominated by contribution from water in the CH_3-covered silica area at the top surface. The presence of the dangling OH peak at 3680 cm^{-1} is characteristic of such an interface.[55] The significantly weaker spectral intensity of the CA ~ 90° case in the bonded OH region compared to the case of bare porous film (Fig. 3) is also expected, knowing that the OTS-covered flat silica surface also has significantly weaker spectral intensity than the bare one. Interfacial water molecules are less polar ordered if they are not hydrogen bonded to the surface. The intensity spectra of the CA ~ 40° appear to be even weaker than those of CA ~ 90°. This could be surprising as one might expect from a partially calcined silica surface that the spectra should have profiles between those of CA = 0° and CA ~ 90°. The result however can be readily understood if we compare the Im $\chi_S^{(2)}$ spectra of water/OTS [Fig. 6(d)] and water/silica interfaces [Fig. 3(d)]. The signs of Im $\chi_S^{(2)}$ in most of the bonded OH

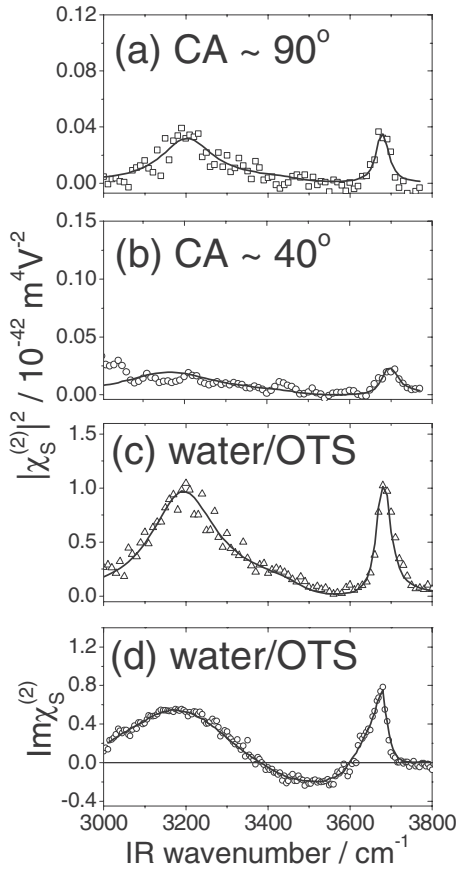

FIG. 6. SSP-$|\chi_S^{(2)}|^2$ spectra of the water/periodic nanoporous silica interface characterized by CAs of (a) 90° and (b) 40° in comparison with (c) the spectrum of the water/OTS interface. (d) SSP-Im $\chi_S^{(2)}$ spectrum of the water/OTS interface.

spectral region of the two spectra are opposite. A linear combination of the two spectra that describes a partially bare and partially silane-covered surface will yield a much weaker spectrum due to cancellation.

B. Fractal nanoporous film

Our fractal nanoporous films were very different from periodic nanoporous films. High porosity led to a surface that is mostly occupied by pores with silica forming a thin network frame. Thus, water molecules in the pore areas of the interface are expected to contribute significantly to the interfacial SFVS spectra of water/fractal porous films.

Figure 7 shows the SSP spectra of $|\chi_S^{(2)}|^2$ and Im $\chi_S^{(2)}$ for the water interfaces with a SH (CA ~ 165°) and a hydrophilic (CA ~ 0°) fractal porous film. Compared with the spectra of water/air and water/silica interfaces also displayed in Fig. 7, the spectrum for the SH film is similar to that of the water/air interface, and the spectrum with the hydrophilic film similar to that of the water/silica interface except for the reduced spectral strength. The former (CA ~ 165°) indicates that air was trapped in the pores at the interface so that the spectrum is dominated by features characteristic of the water/air interface. This is known as the Cassie state of the SH water interface. Note that the dangling OH peak appears at 3700 cm^{-1} as it should. The latter (CA ~ 0°) indicates that water had permeated into the pores (the Wenzel state) so that

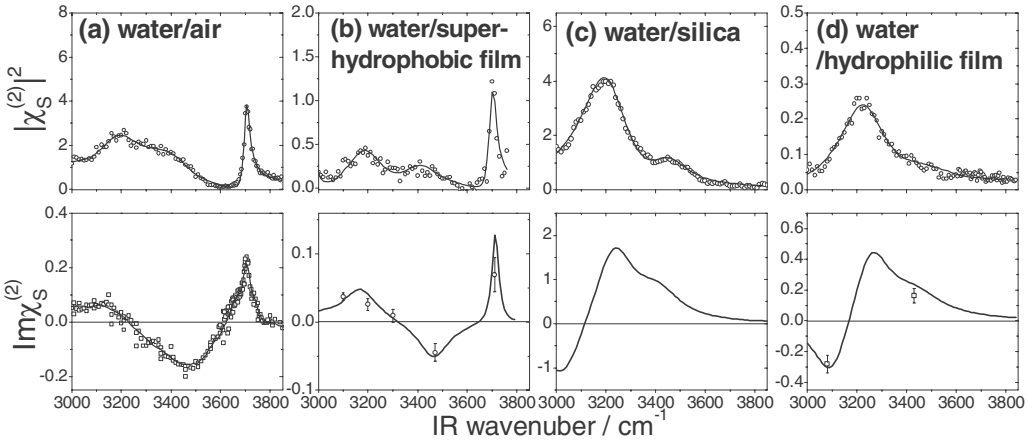

FIG. 7. SSP $|\chi_S^{(2)}|^2$ and Im $\chi_S^{(2)}$ spectra of (a) the water/air interface, (b) the water/SH fractal film interface, (c) the water/fused silica interface, and (d) the water/hydrophilic fractal film interface.

the spectrum is dominated by features characteristic of the water/silica interface including the disappearance of the dangling OH peak. The spectral intensity from the fractal porous surface is however much weaker (~5%) than those of water/air and water/silica interfaces. Presumably, this is the result of orientational average over a wider distribution of molecular species because the water interface at the pores may not be flat, as also evidenced from neutron reflectivity measurements where the water/fractal film interface is determined to be rough.[25] A recent paper on the water/alumina interface[56] also suggests that surface roughness can affect the SFVS water spectrum.

Photocalcination reduced the hydrophobicity of the SH film. Displayed in Fig. 8 is a set of SSP spectra of $|\chi_S^{(2)}|^2$ and Im $\chi_S^{(2)}$ for water interfaces with fractal porous films of different CAs. It shows how the spectrum (Im $\chi_S^{(2)}$ in particular) evolves from the characteristic spectrum of the water/air interface to that characteristic of the water/silica interface. For the partially calcined films, presumably air was still trapped in some of the pores, leading to the continuing presence of the dangling OH peak in the spectrum, although reduced in strength. It is interesting to note that the spectrum does not clearly switch to that characteristic of the water/silica interface until the surface is fully calcined. From Figs. 7 and 8, we can see that when the film becomes hydrophilic, the

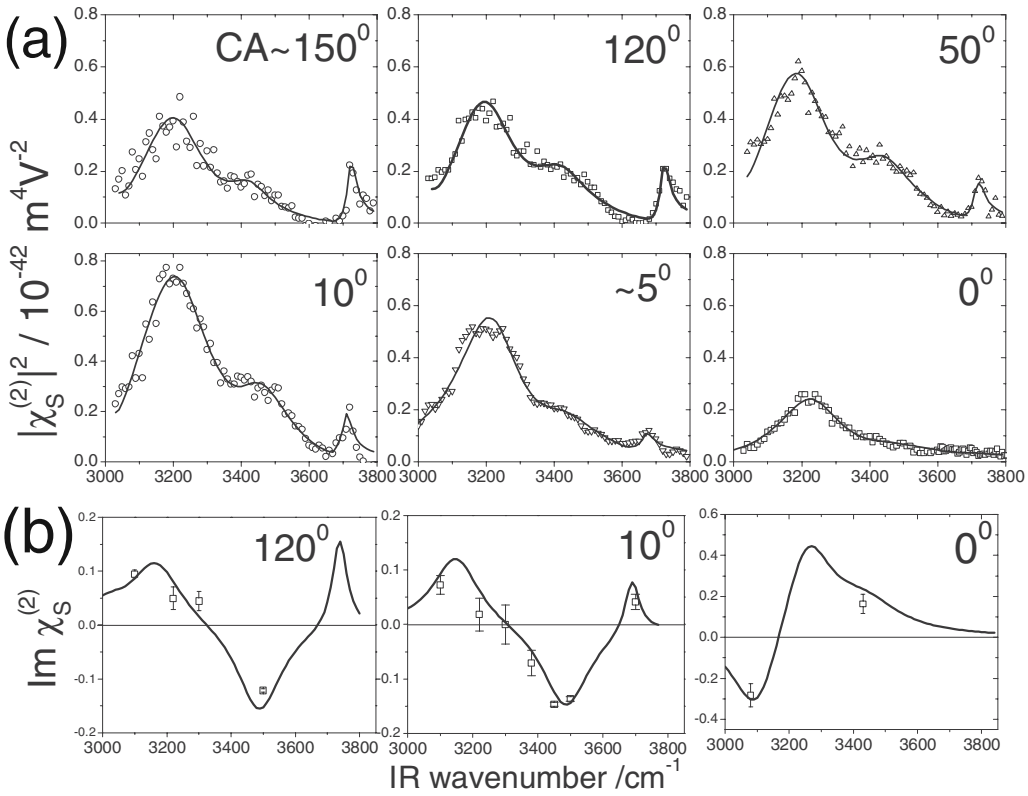

FIG. 8. SSP $|\chi_S^{(2)}|^2$ spectra of water/fractal nanoporous silica interfaces with CAs of (a) 150°, 120°, 50°, 10°, and 0° (hydrophilic surface with no silane coverage) and SSP Im $\chi_S^{(2)}$ spectra of same interfaces with CAs of (b) 120°, 10°, and 0°.

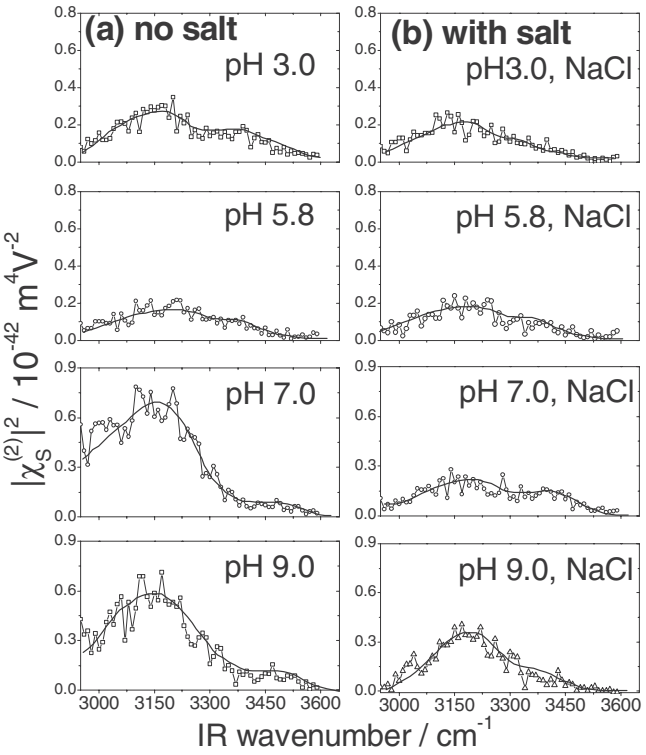

FIG. 9. The *p*H dependence of the SSP spectra for the water/fractal nanoporous silica interface: (a) without electrolyte and (b) with electrolyte (20 mM NaCl aqueous solution). The solid lines are to guide the eyes. The film was not covered by silane.

Im $\chi_S^{(2)}$ spectrum of the water($p\mathrm{H}\sim5.8$)/fractal porous film interface has a significant negative band around 3050 cm^{-1}. This negative band is also present in the spectra of water interfaces with quartz,[28,29] silica [see Fig. 3(d)], and the periodic porous film [see Fig. 4(c)] at lower *p*H but becomes diminishingly small toward $p\mathrm{H}\sim7$. The presence of this negative band for the water/fractal porous film interface even at *p*H 6 suggests that the effect of deprotonation of the fractal porous film is not appreciable at $p\mathrm{H}\sim6$.

We are interested in knowing whether the fully calcined fractal nanoporous silica film has a very different p.z.c. than a flat silica surface. Figure 9 shows a set of SSP spectra for the interfaces of water/fractal film with $\mathrm{CA}\sim0°$ with and without salt in water. The spectrum remains nearly unchanged and unaffected by salt when *p*H increases from 2.0 to 6.0 but becomes significantly stronger afterward and effectible by salt. It is believed that as the surface SiOH groups of the fractal film are deprotonated, the negative surface charges appear randomly on the thin fractal porous network. Because of the high surface porosity, the surface charge density is much less than on a flat silica surface at the same bulk *p*H and less effective in creating a surface field to polar orient the interfacial water molecules. Only when the degree of deprotonation is sufficiently high will the surface field be strong enough to produce detectable polar reorientation of the interfacial water species. This is the case with *p*H above 6, as seen in Fig. 9. The result makes it difficult to determine the p.z.c. for the fractal porous film except to say that it is less than *p*H 6. This corroborates well with the AFM force measurement. As seen in Fig. 5, the effective surface change density becomes clearly nonzero only after the *p*H reaches above *p*H 6.

V. CONCLUSION

Our SFVS study on water interfaces with periodic and fractal nanoporous films provides us with qualitative pictures on water structures at these interfaces. For the periodic nanoporous film we investigated, the top surface was dominated by silica with a 4:1 area ratio with respect to areas occupied by pores. Accordingly, water species adsorbed at the top surface dominated the surface vibrational spectra in all cases. Their structure resembled that of flat water/OTS interface when silica was covered by trimethyl silane (hydrophobic) and resembled that of the flat water/silica interface when silica is bare (hydrophilic). We were not able to determine whether the interfacial water was in the Cassie or Wenzel state because of our inability to identify spectral contribution from water in the pore area. Spectral dependence of the hydrophilic porous surface on *p*H showed that the porous film had a p.z.c. at $p\mathrm{H}\sim2$ similar to that of a flat silica surface. The surface charging behavior with increasing *p*H due to deprotonation was also similar to that of the flat silica surface and agreed qualitatively with results from the AFM force measurements.

For the fractal nanoporous film, there was a bulk porosity of 85% with a corresponding surface porosity of ~90%. When coated by silane, the surface became SH with a CA of 165°. Interfacial water exhibited a spectrum characteristic of the water/air interface, indicating that air was trapped in the pores (the Cassie state). Photocalcination reduced the hydrophobicity and changed the interface to a mixed Cassie–Wenzel state. Finally, the fully calcined surface exhibited a spectrum characteristic of the water/silica interface. Its spectrum was insensitive to *p*H variation below 6, allowing us only to conclude that the p.z.c. of the fractal porous film was in the range of $p\mathrm{H}<6$. The surface charging behavior with increasing *p*H deduced from SFVS results also corroborated well with that deduced from the AFM force measurements. Our study here shows that SFVS could yield useful information on microstructures of water interfaces with nanostructured substrates and on how they vary with hydrophilicity and hydrophobicity.

ACKNOWLEDGMENTS

This work was supported by the NSF Science and Technology Center of Advanced Materials for Purification of Water with Systems (Water CAMPWS; Grant No. CTS-0120978). C.J.B. and S.S. acknowledge the support from Office of Science, U.S. Department of Energy, LDRD program of Sandia National Laboratory, Air Force Office of Scientific Research, and LUNA Innovations.

APPENDIX: DERIVED CHARGE DENSITY FROM AFM FORCE MEASUREMENT

Here we present the raw data of the AFM force measurements and details of the data analysis which lead to Fig. 5 in the text. Figures 10(a)–10(c) show the measured force versus

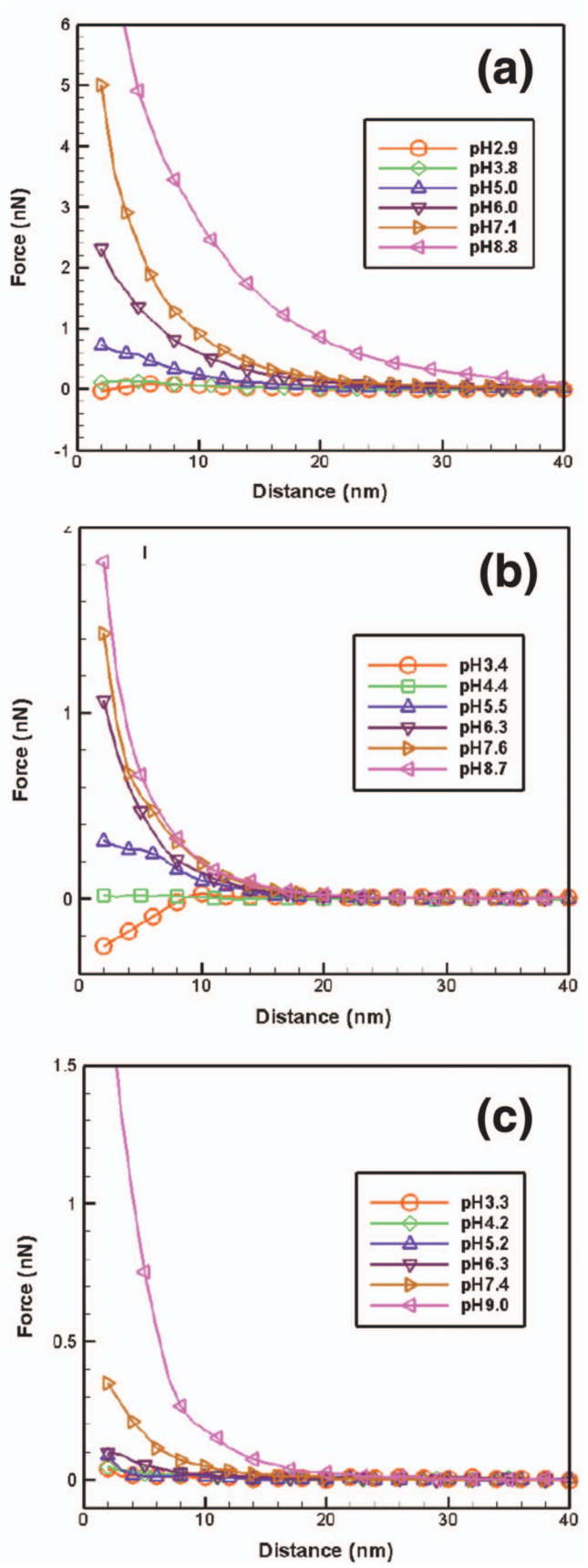

FIG. 10. (Color) Force as a function of tip-sample distance between silica colloidal probe and (a) flat silica surface, (b) periodic nanoporous film, and (c) fractal nanoporous film in aqueous solutions with *p*H ranging from 3 to 9.

distance curves for a fused silica surface, the periodic nanoporous film, and the fractal nanoporous film. Positive and negative forces indicate repulsive and attractive interactions between the probe and sample, respectively.

The force between the probe (a sphere) and the sample (a flat surface) is

$$F = F_{\mathrm{vdW}} + F_{\mathrm{Coul}}, \tag{A1}$$

with F_{vdW} denoting the attractive van der Waals force and F_{Coul} the electric double-layer force, which is always repulsive if the two interacting surfaces are of the same charge polarity and can be attractive if the two surfaces are of opposite charge polarity. The van der Waals force can be expressed as[32]

$$F_{\mathrm{vdW}} = \frac{A_H R}{6D^2}, \tag{A2}$$

where R is the radius of the sphere, D is the distance between the two surfaces, and A_H is the Hamaker constant. In the literature, the Hamaker constant for silica/silica interaction in water has been reported to range from 0.77×10^{-20} to 0.85×10^{-20} J.[32] We used $A_H=0.85\times10^{-20}$ J to estimate F_{vdW} in the following analysis.

Knowing F_{vdW}, we can then deduce F_{Coul} versus D from the measured F versus D for different samples at different *p*H presented in Figs. 10(a)–10(c). The electric double-layer force can be expressed as[32]

$$F_{\mathrm{Coul}} = \frac{2\pi R\lambda_D}{\varepsilon\varepsilon_0}[2\sigma_s\sigma_P e^{-D/\lambda_D} + \sigma_S^2\sigma_P^2 e^{-2D/\lambda_D}], \tag{A3}$$

where σ_s and σ_P are the surface charge densities of sample and probe, and λ_D is the Debye length of the electrolyte solution. Equation (A3) shows that the range of electric double-layer interaction scales with the Debye length.

In order to compare force versus distance curves measured with different solution *p*H, it is important to maintain a constant ionic strength of the solution so that the Debye length stays relative unchanged with titration. For 5 mM NaCl solution titrated from *p*H 3 to *p*H 9, the Debye length ranges from 4.10 (*p*H 3) to 4.30 nm (*p*H greater than 6). We calibrated the surface charge density of the silica colloidal probe as a function of solution *p*H using the measured force curves of the flat silica sample, assuming the probe and sample surfaces have the same charge density at each *p*H and the surface charge density versus *p*H data obeys the basic Stern model described by Behrens and Grier.[57] Knowing σ_P versus *p*H, we can then deduce σ_s versus *p*H for the two nanoporous silica films from F_{Coul} versus D at different *p*H using Eq. (A3). The results are displayed in Fig. 5 in the text.

The above analysis assumes ideal geometry of interactions for the system. Even so, there are limitations on applying Eq. (A3). First, when the electrical double layers of the probe and sample in solution overlap, the surface charge densities of the sample and probe depend on their separation due to the so-called "charge regulation" phenomenon.[57] Second, Eq. (A3) relies on the assumption that the surface charge densities are sufficiently low to warrant for a linearized Poisson–Boltzmann equation. Finally, Eq. (A3) is only valid

for D larger than λ_D.[32] These limitations lead to uncertainty in determination of absolute values of the surface charge densities, which is the reason why we use the term effective charge density in describing the results in Fig. 5. However, with *p*H being the only variable, the relative change in the charge density should still be meaningful.

[1] K. Leung, S. B. Rempe, and C. D. Lorenz, Phys. Rev. Lett. **96**, 095504 (2006).
[2] S. Joseph and N. R. Aluru, Langmuir **22**, 9041 (2006).
[3] A. Zurner, J. Kirstein, M. Doblinger, C. Brauchle, and T. Bein, Nature (London) **450**, 705 (2007).
[4] R. Karnik, R. Fan, M. Yue, D. Li, P. Yang, and A. Majumdar, Nano Lett. **5**, 943 (2005).
[5] R. Fan, S. Huh, R. Yan, J. Arnold, and P. Yang, Nature Mater. **7**, 303 (2008).
[6] G. Wirnsberger, B. J. Scott, and G. D. Stucky, Chem. Commun. (Cambridge) **01**, 119 (2001).
[7] T.-H. C. Yang, C. K. Yee, M. L. Amweg, S. Singh, E. L. Kendall, A. M. Dattelbaum, A. P. Shreve, C. J. Brinker, and A. N. Parikh, Nano Lett. **7**, 2446 (2007).
[8] S. A. El-Safty, D. Prabhakaran, A. A. Ismail, H. Matsunaga, and F. Mizukami, Chem. Mater. **20**, 2644 (2008).
[9] D. Stein, M. Kruithof, and C. Dekker, Phys. Rev. Lett. **93**, 035901 (2004).
[10] A. Lafuma and D. Quere, Nature Mater. **2**, 457 (2003).
[11] Z. Yoshimitsu, A. Nakajima, T. Watanabe, and K. Hashimoto, Langmuir **18**, 5818 (2002).
[12] A. Otten and S. Herminghaus, Langmuir **20**, 2405 (2004).
[13] W. R. Hansen and K. Autumn, Proc. Natl. Acad. Sci. U.S.A. **102**, 385 (2005).
[14] C. Yang, U. Tartaglino, and B. N. Persson, Phys. Rev. Lett. **97**, 116103 (2006).
[15] N. A. Patankar, Langmuir **20**, 7097 (2004).
[16] Y. T. Cheng and D. E. Rodak, Appl. Phys. Lett. **86**, 144101 (2005).
[17] B. Bhushan and Y. C. Jung, Nanotechnology **17**, 2758 (2006).
[18] M. G. Khedr, Desalination **153**, 295 (2003).
[19] M. C. Duke, S. Mee, and J. C. D. da Costa, Water Resour. **41**, 3998 (2007).
[20] S. Singh, J. Houston, F. van Swol, and C. J. Brinker, Nature (London) **442**, 526 (2006).
[21] R. Roth, D. Gillespie, W. Nonner, and R. E. Eisenberg, Biophys. J. **94**, 4282 (2008).
[22] R. N. Wenzel, Ind. Eng. Chem. **28**, 988 (1936).
[23] A. B. D. Cassie and S. Baxter, Trans. Faraday Soc. **40**, 546 (1944).
[24] H. E. Jeong, S. H. Lee, J. K. Kim, and K. Y. Suh, Langmuir **22**, 1640 (2006).
[25] D. A. Doshi, P. B. Shah, S. Singh, E. D. Branson, A. P. Malanoski, E. B. Watkins, J. Majewski, F. V. Swol, and C. J. Brinker, Langmuir **21**, 7805 (2005).
[26] Y. B. Jiang, N. Liu, H. Gerung, J. L. Cecchi, and C. J. Brinker, J. Am. Chem. Soc. **128**, 11018 (2006).
[27] N. Ji, V. Ostroverkhov, C. S. Tian, and Y. R. Shen, Phys. Rev. Lett. **100**, 096102 (2008).
[28] V. Ostroverkhov, G. A. Waychunas, and Y. R. Shen, Chem. Phys. Lett. **386**, 144 (2004).
[29] V. Ostroverkhov, G. A. Waychunas, and Y. R. Shen, Phys. Rev. Lett. **94**, 046102 (2005).
[30] T. Clark, J. D. Ruiz, H. Y. Fan, C. J. Brinker, B. I. Swanson, and A. N. Parikh, Chem. Mater. **12**, 3879 (2000).
[31] A. Hozumi, Y. Yokogawa, T. Kameyama, K. Hiraku, H. Sugimura, O. Takai, and M. Okido, Adv. Mater. (Weinheim, Ger.) **12**, 985 (2000).
[32] H. J. Butt, B. Cappella, and M. Kappl, Surf. Sci. Rep. **59**, 1 (2005).
[33] Y. R. Shen, in *Frontiers in Laser Spectroscopy*, Proceedings of the International School of Physics "Enrico Fermi," Course CXX, edited by T. W. Hansch and M. Inguscio (North-Holland, Amsterdam, 1994).
[34] P. B. Miranda and Y. R. Shen, J. Phys. Chem. B **103**, 3292 (1999).
[35] Z. Chen, Y. R. Shen, and G. A. Somorjai, Annu. Rev. Phys. Chem. **53**, 437 (2002).
[36] X. Wei, P. B. Miranda, and Y. R. Shen, Phys. Rev. B **66**, 085401 (2002).
[37] P. Schiebener, J. Straub, J. M. H. L. Sengers, and J. S. Gallagher, J. Phys. Chem. Ref. Data **19**, 677 (1990).
[38] N. Ji, V. Ostroverkhov, C. Y. Chen, and Y. R. Shen, J. Am. Chem. Soc. **129**, 10056 (2007).
[39] S. W. Ong, X. L. Zhao, and K. B. Eisenthal, Chem. Phys. Lett. **191**, 327 (1992).
[40] B. F. Levine and C. G. Bethea, J. Chem. Phys. **65**, 2429 (1976).
[41] S. Kielich, IEEE J. Quantum Electron. **5**, 562 (1969).
[42] J. P. Fitts, X. M. Shang, G. W. Flynn, T. F. Heinz, and K. B. Eisenthal, J. Phys. Chem. B **109**, 7981 (2005).
[43] L. Zhang, C. S. Tian, G. A. Waychunas, and Y. R. Shen, J. Am. Chem. Soc. **130**, 7686 (2008).
[44] J. Y. Zhang, J. Y. Huang, Y. R. Shen, and C. J. Chen, J. Opt. Soc. Am. B **10**, 1758 (1993).
[45] L. Zhang, W. Liu, Y. R. Shen, and D. G. Cahill, J. Phys. Chem. C **111**, 2069 (2007).
[46] L. Hutter and J. Bechhoefer, Rev. Sci. Instrum. **64**, 1868 (1993).
[47] R. Proksch, T. Schaffer, J. P. Cleveland, R. C. Callahan, and M. B. Viani, Nanotechnology **15**, 1344 (2004).
[48] C. J. Brinker, Y. Lu, A. Sellinger, and H. Fan, Adv. Mater. (Weinheim, Ger.) **11**, 579 (1999).
[49] S. S. Prakash, C. J. Brinker, A. J. Hurd, and S. M. Rao, Nature (London) **374**, 439 (1995).
[50] A. M. Dattelbaum, M. L. Amweg, J. D. Ruiz, L. E. Ecke, A. P. Shreve, and A. N. Parikh, J. Phys. Chem. B **109**, 14551 (2005).
[51] A. M. Dattelbaum, M. L. Amweg, L. E. Ecke, C. K. Yee, A. P. Shreve, and A. N. Parikh, Nano Lett. **3**, 719 (2003).
[52] J. J. Sagiv, J. Am. Chem. Soc. **102**, 92 (1980).
[53] The three discrete bands used in our analysis are an approximation of the continuum resonances in the OH stretching region. They yield Im $\chi_S^{(2)}$ spectra nearly the same as those obtained directly from measurement, as seen in Refs. 27 and 29.
[54] Y. Duval, J. A. Mielczarski, O. S. Pokrovsky, E. Mielczarski, and J. J. Ehrhardt, J. Phys. Chem. B **106**, 2937 (2002).
[55] S. Ye, S. Nihonyanagi, and K. Uosaki, Phys. Chem. Chem. Phys. **3**, 3463 (2001).
[56] B. Braunschweig, S. Eissner, and W. Daum, J. Phys. Chem. C **112**, 1751 (2008).
[57] S. H. Behrens and D. G. Grier, J. Chem. Phys. **115**, 6716 (2001).